Photochemical and Discharge-Driven Pathways to Aromatic Products from 1,3-Butadiene

Josh J. Newby, Jaime A. Stearns,† Ching-Ping Liu, and Timothy S. Zwier*

Department of Chemistry, Purdue University, West Lafayette, Indiana 47907-2084

Received: July 5, 2007; In Final Form: August 9, 2007

A detailed study of the photochemical and discharge-driven pathways taken by gas-phase 1,3-butadiene has been carried out. Photolysis or discharge excitation was initiated inside a short reaction tube attached to the outlet of a pulsed valve. Bath gas temperatures near 100 K were achieved in the reaction tube by the constrained expansion of the gas mixture into the tube, simulating temperatures of relevance in Titan's atmosphere. Photolysis of 1,3-butadiene was initiated at 218 nm with a laser pulse that counter-propagated the reaction tube. Discharge excitation was carried out using discharge electrodes imbedded in the reaction tube walls, enabling the study of the photochemical and discharge products under similar conditions. Products were detected using either single-photon VUV photoionization (118 nm = 10.5 eV) or resonant two-photon ionization (R2PI) spectroscopy in a time-of-flight mass spectrometer. Emphasis was placed on characterization of the aromatic products formed, since these may be of particular relevance to Titan's atmosphere, where benzene has been positively identified and 1,3-butadiene is projected as the principle pathway to its formation. Consistent with previous studies of the photodissociation of 1,3-butadiene, $C_3H_3 + CH_3$ is the dominant primary product formed. Under the temperature−pressure conditions present in the reaction tube ($T \sim 75-100$ K, $P = 50$ mbar), C_6H_6 is the dominant secondary photochemical product formed. A 1:1 C_4H_6:C_4D_6 mixture was used to prove that the C_6H_6 product was formed by recombination of two C_3H_3 radicals; however, a careful search for benzene revealed none, indicating that less than 1% of the C_6H_6 formed in the reaction tube is benzene. This is consistent with expectations for these temperatures and pressures based on previous modeling of propargyl recombination. Two aromatic products were observed from the photochemistry: ethylbenzene and 3-phenylpropyne. Plausible pathways leading to these products are proposed. In the discharge, $C_3H_3 + CH_3$ are also identified as significant primary neutral products and C_6H_6 as a dominant higher-mass product. In this case, the C_6H_6 was identified as benzene via its R2PI spectrum, appearing with intensity about 10 times larger than any other aromatic formed in the discharge. R2PI spectra of a total of about 15 aromatic products were recorded from the 1,3-butadiene discharge, among them toluene; styrene; phenylacetylene; *o*-, *m*-, and *p*-xylene; ethylbenzene; indane; indene; β-methylstyrene; and naphthalene. Previously unidentified spectra in the *m*/*z* 142 and 144 mass channels were positively identified as the 1,3- and 1,4-isomers of phenylcyclopentadiene and the analogous 1-phenylcyclopentene.

I. Introduction

The dense haze observed on Saturn's moon Titan has been the source of much previous investigation stretching over many years.[1−7] With the arrival of the Cassini−Huygens spacecraft in early 2005, there has been a deluge of new, quantitative data on the conditions and composition of the atmosphere and cloud formation occurring on this unique planetary body.[8−11]

The rich array of hydrocarbons present in Titan's atmosphere is thought to be formed primarily by photochemical processing by solar radiation.[12−15] Aromatic molecules are considered by current photochemical models as important large-molecule components of the atmosphere and are thought to be likely contributors to the visible-absorbing material present in the thick haze that shrouds the moon's surface.[5,7,16] Recent data from the Huygens probe has confirmed the presence of benzene in the atmosphere of Titan,[17] raising the prospect that many larger aromatic derivatives and polyaromatic hydrocarbons (PAH) will also be important atmospheric constituents that could contribute to the visible-absorbing haze. The recent study by Waite et al.[18] provides evidence that ion−molecule reactions in the ionosphere may play a significant role in producing large hydrocarbons, including aromatics, but this new pathway is thought to be a supplement to the neutral pathways that occur at lower altitudes.[12,18]

For these reasons, the photochemical pathways leading from small hydrocarbons to benzene, the prototypical aromatic, are especially important to understand. Current photochemical models of the outer planets' atmospheres focus on the recombination of propargyl radicals as the primary pathway to benzene. By comparison, other reaction pathways, such as the reaction between metastable diacetylene and butadiene, or hydrogen addition to phenyl radical, are considered to be relatively minor.[15,16] As a result, understanding the sources and sinks of the propargyl radical in Titan's atmosphere is crucial.

Photolysis of 1,3-butadiene is predicted by the models to be the dominant source of propargyl on Titan.[15,16] Upon photoexcitation to the 1 ^1B_u state around 220 nm, 1,3-butadiene is known to undergo rapid internal conversion to the ground state, leaving several energetically available dissociation and isomerization pathways.[19] Molecular beam experiments have confirmed that

* Author to whom correspondence should be addressed. E-mail: zwier@purdue.edu.

† Present address: Laboratoire Chimie Physique Moléculaire, Ecole Polytechnique Fé dérale de Lausanne, CH-1015 Lausanne, Switzerland.

10.1021/jp0752567 CCC: $37.00 © 2007 American Chemical Society
Published on Web 10/11/2007

propargyl radical is the major product of photolysis of 1,3-butadiene or 1,2-butadiene at 193 nm,[19,20] photolysis of 1,3-butadiene at 157 nm,[21] and pyrolysis of 1,2- or 1,3-butadiene at temperatures up to 1500 K.[22] A comprehensive ab initio study of the C_4H_6 potential energy surface (PES) and solution of the kinetics and product yields via RRKM based master equation analysis gave product yields in good agreement with the experimental 193 nm photolysis data.[23]

While the photochemistry[24−26] and dissociation[19,20] of 1,3-butadiene have been studied in some detail, much less is known about the subsequent fate of the primary products, particularly propargyl radicals, under conditions relevant to Titan's atmosphere. In Titan's atmosphere, temperatures range from 70 to 150 K and pressures from 50 to 100 mbar in the regions where photochemical production of propargyl occurs most efficiently.[15,27]

One major purpose of this work is to carry out studies of the photochemistry of 1,3-butadiene and follow the subsequent propargyl reactions at conditions nearer to those in Titan's atmosphere. The present study on 1,3-butadiene is part of a larger effort to search for new photochemical pathways to aromatic ring formation. Much of our previous effort was directed at studies of diacetylene (C_4H_2), which forms metastable triplet states following ultraviolet excitation. We have studied the chemistry of metastable diacetylene with a range of hydrocarbons present in Titan and the outer planets' atmospheres.[24,28−30] In one such study, it was shown that metastable diacetylene reacts with butadiene to produce benzene ($+C_2H_2$) and phenylacetylene ($+H_2$) as photoproducts.

Propargyl recombination occurs on a C_6H_6 potential energy surface that is quite complicated.[31,32] Direct recombination of two propargyl radicals necessarily forms a linear C_6H_6 adduct, and significant rearrangement is required to form benzene. Depending on the temperature and pressure under which the experiment is carried out, the C_6H_6 adduct could be stabilized in any of the several C_6H_6 isomer minima found on the ground state C_6H_6 surface. Miller and Klippenstein carried out simulations that predicted that at lower temperatures ($T < 500$ K) and pressures similar to those found in photochemically active regions of Titan's atmosphere, benzene formation was small and products of C_3H_3 recombination were generally trapped in the other product well (1,5-hexadiyne, 3,4-dimethylenecyclobut-1-ene).[31,32] Kinetics and product analyses of Shafir et al. from laser photolysis of propargyl precursors also show that benzene does not become a major product until the temperature is well above 500 K.[33] As we shall see, a major finding of the present study is that, under the conditions of our experiment, no measurable benzene is formed from propargyl recombination.

At the same time, while benzene is often earmarked as the singular starting point for aromatic chemistry by virtue of its prototypical aromatic structure, other aromatic derivatives may play roles of similar or greater importance. The present study includes a careful search for other aromatic derivatives formed by secondary or higher-order reactions of photoexcited butadiene.

The other major focus of the present study is a comparison of the photochemistry of 1,3-butadiene with its discharge-driven chemistry carried out under similar conditions of temperature and pressure. The history of laboratory studies of relevance to Titan's atmosphere is replete with studies of discharge-driven chemistry leading to "tholins", which have been advocated as a close analog for the physical properties of the aerosol haze material in Titan's atmosphere.[4,34−36] One of our goals here is to directly compare the complex molecules, particularly aromatics, formed in a discharge to those formed by photochemical pathways. Unlike most previous studies that focus only on the macroscopic material formed after repeated exposure of gas mixtures to an electric discharge, the present study characterizes the products formed after exposure to a single, 10 μs long pulsed discharge.

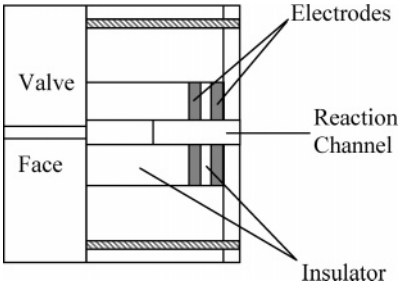

Figure 1. Cut-away view of the reaction tube used for photochemistry and discharge experiments. Opposing high potentials are applied to the electrodes as the gas pulse passes between the electrodes in order to initiate an electric discharge.

II. Experimental Section

Photochemical studies have been conducted in a vacuum chamber designed expressly for sensitive and structurally specific detection of the early time products.[37] Target molecules are introduced to the vacuum chamber diluted in a carrier gas through a pulsed valve (R. M. Jordan Co.) operating at 20 Hz. The gas mixture of interest (3−6% butadiene in argon) is pulsed from a reservoir into a reaction tube (~2 mm diameter × 2 cm long). The gas pulses traverse the reaction tube before collisions are quenched as the gas mixture expands into the vacuum chamber. The number density can be calculated from the flow rates (typically 1.5 mbar·cm^3/pulse), the volume of the reaction tube (2 mm diameter × 2 cm long), the length of the gas pulse (60 μs), and the transit time through the reaction tube (60 μs). From these, a total number density of roughly 5×10^{16} molecules/cm^3 inside the reaction tube, equivalent to a pressure of 50 mbar, is predicted. The temperature inside the reaction tube under these operating conditions has been determined previously to be 75−100 K.[38] By comparison, Titan's atmosphere ranges from 70 to 150 K and pressures from 10 to 100 mbar over the altitude range from the tropopause (50 km) to the upper stratosphere (150 km).[27]

Photochemical reactions are initiated by firing an ultraviolet excitation laser into the reaction tube (Figure 1), timed to intersect the gas pulse while it is in the tube.

Throughout this work, 218 nm light is used as the butadiene photodissociation wavelength, a compromise between efficient absorption and ease of generation of the required wavelength. An unseeded Nd:YAG pumped KTP/BBO optical parametric oscillator/optical parametric amplifier (LaserVision) is used as the photoexcitation laser. This system operates at a power of ~0.2 mJ per pulse at 218 nm.

Alternatively, pulsed electrical discharge generation of intermediates is initiated by applying opposing, high-voltage pulses (±500 V) to the electrodes contained in the reaction source (Figure 1). This discharge source was based on the design of Reid,[39] Clouthier,[40] and Maier.[41] As the gas pulse reaches the discharge region, an electrical arc is initiated between two ring electrodes that are separated by 1 mm. The duration of the arc can be controlled using a fast, high-voltage circuit, allowing for discharges of 1−100 μs duration. The opposing potentials are generated using a high-voltage pulse modulator (DEI model PVM-4210). This generator is tunable from 0 to 950 V for each

polarity, offering a total potential difference of up to 1900 V. Typical operating conditions use ±500 V on the electrodes, as the discharge becomes increasingly unstable at voltages less than ±400 V. The discharge current is regulated by a ballast resistor (10 kΩ) to a peak current of 100 mA. Since the high voltage electrodes are incorporated into the reaction channel, photochemistry and discharge chemistry experiments can be performed under similar conditions without changes to the valve setup. The discharge plates are capped with a 1 mm thick plate that was kept at this minimum length in order to look at early time discharge products.

After molecules leave the reaction tube, they are cooled by further expansion to a temperature of a few kelvin and enter the ion-source region of a Wiley−McLaren time-of-flight vacuum chamber. A laser beam intersects the expansion where reaction products are ionized. Once ionized, these molecules are accelerated down the time-of-fight stage and detected by means of a microchannel plate (MCP) ion detector. The signal generated by the MCP is recorded as a function of time on a digital oscilloscope and is transformed into a mass spectrum.

Product signals in the photochemistry experiments are typically a few percent of the parent ion signal. In order to enhance sensitivity to products, a fast ion gate pulser is used to pulse away the parent signal.[38] When the pulser is switched on, ions are selectively deflected away from the detector. By using fast electronics, it is possible to selectively remove the reactant signal, while product signals are retained only one mass unit away. The mass gate pulser is based on the design of Vlasak et al.[42] High voltage is supplied using a high-voltage pulse modulator (DEI model PVM-4210) with nanosecond rise times.

In the ion source, reactive intermediates, and secondary reaction products can be detected by several ionization schemes. These schemes include vacuum ultraviolet (VUV) photoionization, ultraviolet multiphoton ionization (UVMPI), and resonant two photon ionization (R2PI). VUV light is generated by tripling the third harmonic of a Nd:YAG laser to produce 118 nm light (10.5 eV).[29,43] VUV ionization allows for ionization of molecules with ionization potentials (IP) below 10.5 eV, typically with minimal fragmentation. As a result, 118 nm VUV photoionization provides an overview of the primary and secondary products formed. Since one of our major interests is in pathways that lead to aromatics, UVMPI is used to enhance their detection, using 266 nm light (∼1 mJ/pulse) from the fourth harmonic of the Nd:YAG laser. Since aromatics typically absorb at or near this wavelength and have ionization potentials low enough to be reached by two-photon excitation (9.3 eV), their detection is selectively enhanced. In this sense, UVMPI provides a first indicator of the masses that one should probe in more detail using R2PI spectroscopy. However, the fixed wavelength can skew the ion abundances toward species that most strongly absorb at 266 nm.

R2PI spectra are recorded using the tunable output of a frequency-doubled, Nd:YAG-pumped dye laser. In order to search the relevant wavelength ranges where aromatic products are typically observed, spectra were recorded using dyes that cover the 650−420 nm region, including Rhodamine 610, 575, 6G; Fluorescein 548; and Coumarin 540, 503, and 440. An R2PI spectrum is recorded by plotting the change in ion signal in a given mass channel as a function of laser wavelength. This spectrum is the UV spectrum of the molecule, which is also a signature of the molecular structure, often leading to unambiguous assignments of the carrier of the spectrum. R2PI spectra of discharge products were generally recorded as 128 or 256 shot averages with a step size of 0.03 nm. Due to the low signal intensities observed in discharge experiments, it was necessary to increase the laser power to the point that many of the strong transitions are saturated (0.3−0.5 mJ/pulse). When reference spectra are acquired from neat samples, R2PI spectra were generally recorded as 32 shot averages at 0.01 nm per step with somewhat lower laser powers where the transitions were less saturated (<0.2 mJ/pulse).

One of the particular challenges of the complex chemistry leading to aromatic products is that the products can include structural and conformational isomers with the same molecular formula. UV−UV hole-burning (UVHB) spectroscopy is then used to dissect the R2PI spectra in a given mass channel into individual spectra due to each isomeric product. In UVHB experiments, a hole-burn laser, operating at 10 Hz, is fixed on a strong transition in the R2PI spectrum. Its power (∼0.5 mJ/pulse) is sufficient to saturate or partially saturate this transition, thereby removing a measurable fraction of the ground state population of this species. A probe laser, spatially overlapped with the hole-burn laser and operating at 20 Hz, is delayed from the hole-burn laser by 50−500 ns. The probe laser wavelength is then tuned through the ultraviolet spectral region of interest, while the difference in signal between successive probe laser pulses is recorded using active baseline subtraction through a gated integrator. When the probe laser is resonant with a transition that shares the same ground state level as the transition that is being pumped by the hole-burn laser, a nonzero difference signal is detected. The UVHB spectrum thus detects only transitions from the species "tagged" by the hole-burn laser.

III. Results and Analysis

A. Photochemistry. Figure 2 presents VUV difference time-of-flight mass spectra of a 6% 1,3-butadiene in argon mixture following photoexcitation at 218 nm. Figure 2a depicts the portion of the spectrum with masses below that of the parent 1,3-butadiene (*m/z* 54) due to primary photodissociation products, while Figure 2b presents a higher mass region due to secondary reaction products.

The small, negative-going peaks in the difference mass spectra are due to incomplete subtraction of the ion signal from several minor impurities in the sample. These peaks are negative because of small changes in the transport of the gas mixture into the ion source region in the presence of the photoexcitation laser.[24] The spectra were recorded by coadding the ion signal from 512 laser pulses in the presence of the photodissociation laser and subtracting the ion signal from an analogous coadded scan taken in the absence of the photodissociation laser. The primary photodissociation products are consistent with those observed in previous studies,[19−21] keeping in mind that only products with ionization potentials below 10.5 eV will be observed: CH_3, C_3H_3, C_4H_4, and C_4H_5. Note the efficient removal of the reactant C_4H_6 ion signal with the mass gate pulser, enabling detection of photodissociation products only a single mass unit away, even though they are more than 100 times smaller in size in the absence of the pulser. The photodissociation processes responsible for these primary products are

$$(C_4H_6) + h\nu \rightarrow C_3H_3 + CH_3 \quad (1a)$$

$$\rightarrow C_4H_4 + H_2 \quad (1b)$$

$$\rightarrow C_4H_5 + H \quad (1c)$$

The relative intensities of the primary product peaks in the difference mass spectrum are determined by the relative

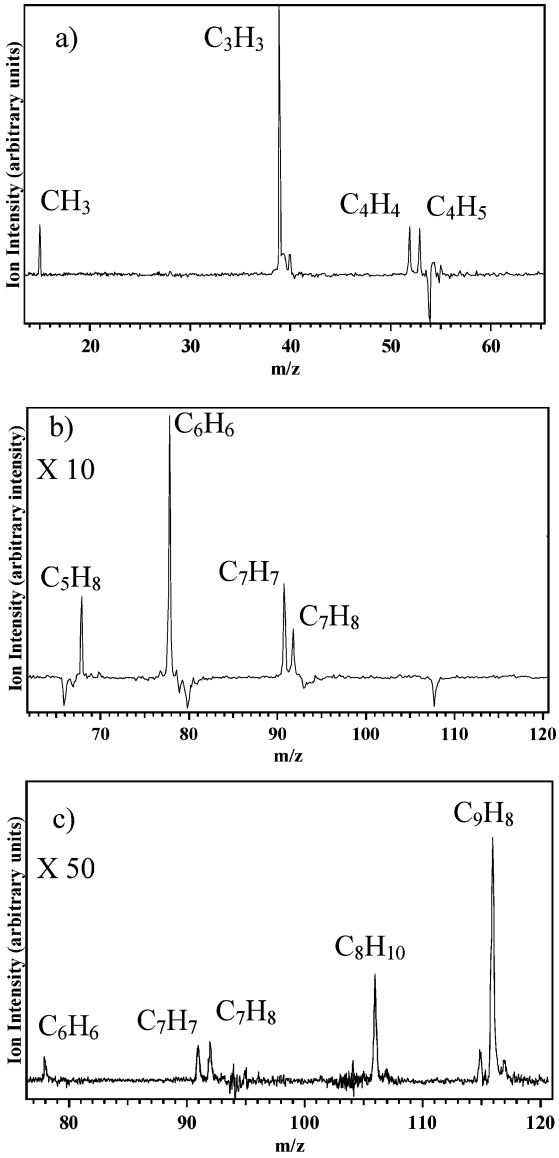

Figure 2. (a) Difference mass spectra of butadiene primary photoproducts excited at 218 nm and detected by VUV ionization. (b) Difference mass spectra of butadiene secondary photoproducts detected via VUV ionization. (c) Difference mass spectra of butadiene secondary photoproducts detected via UVMPI, taken with a collimated, 1 mJ/pulse 266 nm laser beam.

photodissociation quantum yields and the ionization cross sections of each at 118 nm. Since the C_3H_3 and CH_3 products are necessarily formed in a 1:1 ratio, their relative intensities reflects their relative photoionization cross sections at 118 nm. On the basis of the known cross section for propargyl (8.5 Mb),[44] we deduce a photoionization cross section for methyl radical of 1.1 Mb. The analogous cross sections for C_4H_4 and C_4H_5 products are not known at 118 nm, preventing the determination of primary product quantum yields from the observed product intensities. Furthermore, since the ionization potentials of their dissociation partners (H_2 and H respectively) are above 10.5 eV, the cross sections of the two C_4 products cannot be estimated.

An important goal of the present study is to follow the subsequent reactions of these primary products with each other and with the 1,3-butadiene precursor. Figure 2b presents a VUV difference time-of-flight mass spectrum of the mass channels greater than the reactant. Among the observed mass products

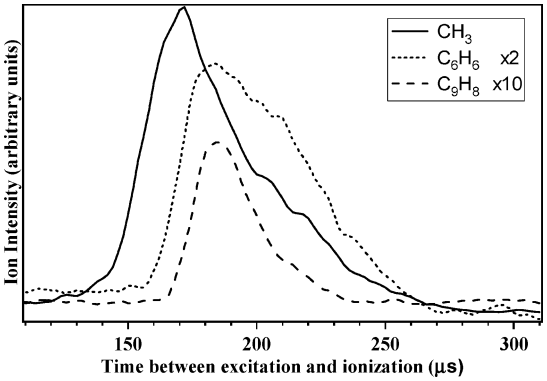

Figure 3. Ion signals of photoproducts as a function of time between excitation and ionization. Solid trace: primary photoproduct signal (CH_3). Dotted trace: secondary product (C_6H_6). Dashed trace: aromatic secondary product (C_9H_8).

are peaks at m/z = 68, 78, 91, and 92, which are associated with hydrocarbon products of molecular formulas C_5H_8, C_6H_6, C_7H_7, and C_7H_8. The secondary product signals (Figure 2b) are about 10 times smaller than those due to primary products (Figure 2a), consistent with the short reaction time associated with the present experimental arrangement. Figure 2c shows a difference spectrum taken with UVMPI at 266 nm, which enhances detection of aromatic products. Interestingly, this spectrum is dominated by peaks at m/z = 106 and 116, corresponding to C_8H_{10} and C_9H_8 products, respectively. While the C_8H_{10} product could be formed by reaction of the C_4H_4 or C_4H_5 primary product with butadiene, the C_9H_8 product must be a higher-order product associated with subsequent steps that follow the first radical−molecule or radical−radical reaction.

One helpful diagnostic of the sequence of reactions follows from recording scans of product ion signals as a function of the delay time between the photoexcitation and VUV laser pulses. Because the photoexcitation laser counter propagates the reaction tube, it produces a column of primary products that can subsequently react during the remainder of their traversal down the reaction tube. In the limit of plug flow, lengthening the delay between the pulses is equivalent to changing the position of excitation along the reaction tube probed by the VUV laser. As a result, these scans are called "reaction time" scans in what follows.

During the traversal of the reaction tube, the radicals created by photolysis of butadiene are estimated to undergo hundreds of collisions with the buffer gas, tens of collisions with the parent molecule, and a few collisions with other radicals. Reactive collisions result in formation of secondary products. Figure 3 presents a series of reaction time scans monitoring the CH_3^+, $C_6H_6^+$, and $C_9H_8^+$ mass channels.

The onsets for the three products follow the anticipated order of their formation, with CH_3 showing the earliest onset, followed by C_6H_6 as a secondary product and C_9H_8 as a tertiary product. The C_6H_6 secondary reaction product also has a somewhat different shape to its distribution at late times, showing a preferential enhancement at late times. Analogous scans taken with helium as buffer gas (not shown) confirm that all primary products are peaked toward earlier time, while the secondary products are characteristically peaked later, but have a narrower time profile with a cutoff at similar delays to the primary products. This long-time cutoff is affected by the length of the gas pulse (∼60 μs) and the quenching of the reaction as the gas mixture exits the reaction tube.

Since C_3H_3 is the most abundant primary photoproduct (Figure 2a) and C_6H_6 is the most prevalent secondary product

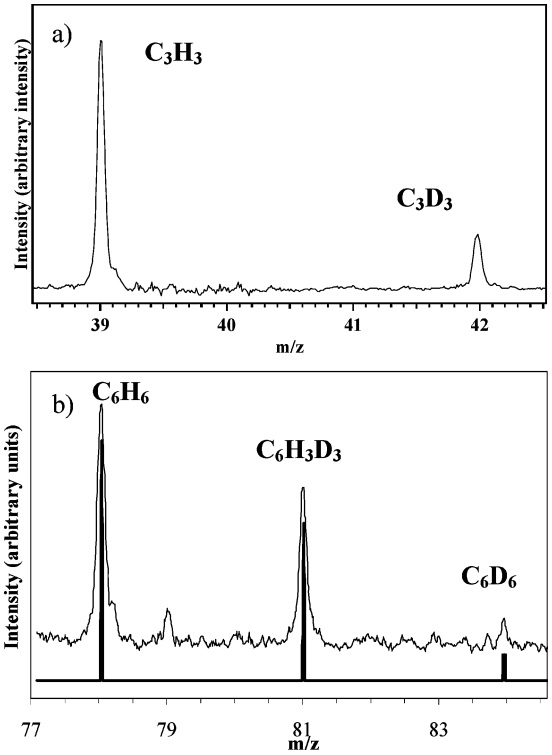

Figure 4. 118 nm photoionization difference time-of-flight mass spectra of (a) the initial 4.3:1 C_3H_3:C_3D_3 mixture of isotopomers formed by 218 nm photolysis of a 1:1 mixture of C_4H_6:C_4D_6. (b) The analogous isotopic distribution of C_6H_6 products formed by propargyl recombination. The bar graph gives the prediction of statistical recombination of the propargyl isotopomers.

(Figure 2b) observed, it is natural to assume that propargyl recombination is a dominating mechanism for C_6H_6 formation:

$$2C_3H_3 + M \rightarrow C_6H_6 + M \tag{2a}$$

However, other reactions, such as those between C_3H_3 or C_4H_5 and parent 1,3-butadiene, also have exothermic pathways (see Supporting Information) to some isomeric C_6H_6 products and thus could, in principle, be involved:

$$C_3H_3 + C_4H_6 \rightarrow C_6H_6 + CH_3 \tag{2b}$$

$$C_4H_5 + C_4H_6 \rightarrow C_6H_6 + C_2H_5 \tag{2c}$$

Of these possibilities, the recombination of propargyl radicals (reaction 2a) will display a unique isotopic signature in the C_6H_6 products that reflects the isotopic composition of the C_3H_3 primary products formed in the photodissociation. For example, if photodissociation of an isotopic mixture of C_4H_6 and C_4D_6 produces a 50:50 mixture of C_3H_3:C_3D_3, then, barring significant kinetic isotope effects, one would expect a 1:2:1 mixture of C_6H_6:$C_6H_3D_3$:C_6D_6 to be produced.

To that end, we prepared a 50:50 mixture of butadiene(h_6): butadiene(d_6) and recorded VUV difference mass spectra following photodissociation at 218 nm. Identical conditions were used to those in the photochemistry experiments just described. VUV ionization of the mixture in the absence of the photoexcitation laser confirmed that the mixture prepared did indeed consist of nearly equal concentrations of C_4H_6 and C_4D_6. Surprisingly, the intensity ratio of the C_3H_3:C_3D_3 primary products was not 50:50 but 81:19 (Figure 4a). This skewing of the propargyl distribution relative to the parent can be rationalized by the difference in the absorption spectra of butadiene-(h_6) and butadiene(d_6) at 218 nm. Even in a jet-cooled environment, the 1 $^1B_u^+ \leftarrow$ 1 $^1A_g^-$ transition of butadiene (and butadiene-d_6) is quite broad.[45] However, 218 nm is on the long wavelength edge of this absorption, where the absorption cross section is quite sensitive to small changes, and the absorption cross section of C_4D_6 is about half that of C_4H_6 at our excitation wavelength (218 nm).

When the time delay between photoexcitation and VUV laser pulses is moved to the maximum for secondary product formation, only three isotopomers of C_6 are observed (Figure 4b), C_6H_6, $C_6H_3D_3$, and C_6D_6, as one would anticipate if propargyl recombination were responsible for the observed products. Furthermore, the observed product distribution (0.61: 0.35:0.03) is in excellent agreement with that predicted for a statistical distribution of products produced by propargyl recombination from an 0.81:0.19 mixture:

$$(0.81)^2{:}2(0.81)(0.19){:}(0.19)^2 = 0.66{:}0.31{:}0.04$$

By comparison, even in the limit that the $C_3H_3 + C_4H_6$ reaction produced the same isotopic combination of products in a statistical ratio, we would anticipate a 0.81:1.00:0.19 isotopic ratio (0.40:0.50:0.10 product yield), in significant disagreement with what is observed.

Having determined that the C_6H_6 products arise from propargyl recombination, it is important next to determine whether the C_6H_6 product formed under the low-temperature conditions of the reaction tube is benzene. This seems unlikely, given the very small C_6H_6 signal obtained at 266 nm (Figure 2c), a wavelength close to the S_0-S_1 transition of benzene. However, the fixed wavelength used makes it likely that resonant excitation is not achieved.

Using R2PI spectroscopy, a careful search for benzene was carried out using the 6^1_0 band of benzene as diagnostic. A very weak signal due to benzene was found, very near our detection limit. From observed signal intensities of benzene under VUV and R2PI conditions, we estimate that less than 1% of the observed C_6H_6 in Figure 2b can be ascribed to benzene. Unfortunately, none of the large number of possible nonaromatic C_6H_6 isomers have known or well-resolved ultraviolet spectra,[46,47] making it unlikely that R2PI spectroscopy could be used to identify the isomers that are formed. As a result, we did not pursue such scans. For similar reasons, we did not search for any spectroscopic signatures of the C_5H_8 product, which cannot be aromatic.

The C_7H_8 product has the molecular formula of toluene; hence, we probed its S_0-S_1 origin transition in R2PI spectroscopy. Again, only a very weak signal due to toluene was observed, very near the detection limit. On the basis of this signal, we estimate that ~1% of the C_7H_8 signal can be ascribed to toluene. An analogous search for benzyl radical (C_7H_7) via its S_0-S_1 transition was not carried out.

Instead, the small signals at *m/z* 106 (C_8H_{10}) and 116 (C_9H_8) that appeared in the UVMPI spectrum (Figure 2c) were interrogated by R2PI spectroscopy. In both cases, sharp transitions were observed, although with very weak intensity sufficient only for identification. By comparing the observed spectrum with literature UV spectra of C_8H_{10} isomers,[48] the *m/z* 106 product was identified as ethylbenzene, while the corresponding transitions due to the structural isomers of xylene were not detected. The spectrum in the *m/z* 116 mass channel (C_9H_8) did not match any spectra found in the literature. However, we recorded the jet-cooled R2PI spectrum of a purchased sample of 3-phenyl-1-propyne (3PP) and found that it matched the C_9H_8

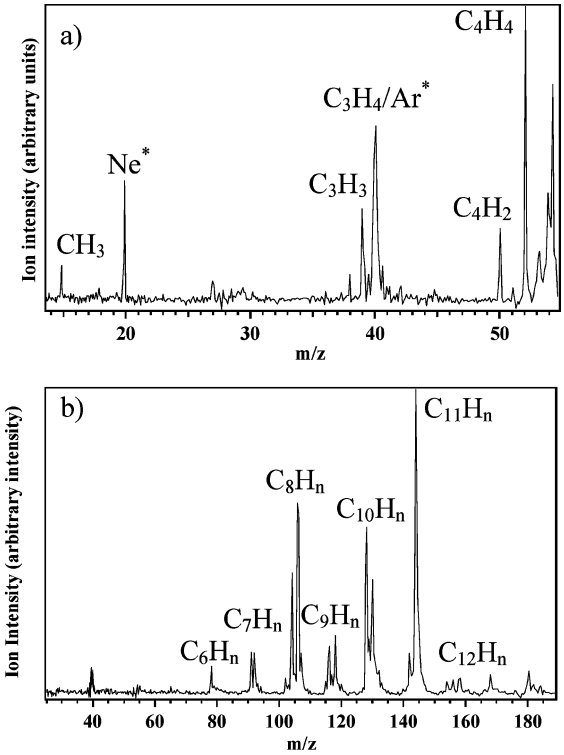

Figure 5. (a) Difference mass spectra recorded from the butadiene discharge using VUV ionization at 118 nm and (b) 266 nm UVMPI to enhance detection of aromatic products.

photoproduct spectrum, thereby identifying it as such. We will consider possible pathways to these products in the Discussion section.

B. Discharge. In order to compare the products and pathways of photochemical and discharge-driven pathways under similar conditions, we have carried out an analogous study of the products formed following pulsed discharge excitation of 1,3-butadiene. In this case, argon was used exclusively as the buffer gas in the reaction mixture, because it facilitated a more stable discharge than helium due to its lower ionization potential. As Figure 5a shows, only weak signals were detected using VUV photoionization in the time-of-flight mass spectrum, those only of smaller neutral products including CH_3, C_3H_3, C_4H_2, and C_4H_4.

The CH_3, C_3H_3, and C_4H_4 products are the same ones that dominate the primary photochemical products (Figure 2a), though they appear from the discharge with quite different relative intensities. The possible presence of C_4H_5 is masked by a larger interference around the butadiene parent mass arrival time. The ion signals at *m/z* 40 and 20 probably arise from Ar and Ne atoms (the latter present as an impurity in the Ar buffer) formed in metastable neutral states in the discharge, with energies sufficiently high that they can be ionized with 118 nm (10.5 eV) light.

Figure 5b shows the corresponding 266 nm UVMPI difference mass spectrum from the discharge. The contrast with the analogous spectrum using ultraviolet excitation (Figure 2c) is striking. With the discharge, a much wider range of product masses are observed, with signal sizes about twice the intensity of the most intense photochemical products. The product masses with significant intensity begin at *m/z* 78 ($C_6H_6^+$) and end near *m/z* 180 ($C_{14}H_n$).

Armed with this knowledge about the masses of potential aromatic products formed in the discharge, we carried out an extensive study of the R2PI spectra of the mass channels up through *m/z* 144, which captures the majority of the product ion intensity in Figure 5b). R2PI scans in this mass range were recorded over wavelength ranges of relevance to the products of interest, with coverage from 32 000 to 40 000 cm^{-1} (310−250 nm). In the case of benzyl radical, an R2PI scan was taken with the resonant step tuned over the 455−430 nm region. When scanning R2PI spectra in search of transitions at longer wavelengths than 266 nm, two-color R2PI was used in order to be sure that the second photon is always energetic enough to ionize. In all spectra recorded here, the second photon was at 266 nm (∼0.2 mJ/pulse).

TABLE 1: Identified Mass Channels in the Discharge Chemistry Experiments with the Observed Wavenumber Position of the S_0-S_1 Origin Transition

m/z	molecular formula	identity	origin (cm^{-1})[d]	literature (cm^{-1})	ref
78	C_6H_6	benzene	38 616	38 612[a]	49
91	C_7H_7	benzyl radical	22 003	22 000	50
92	C_7H_8	toluene	37 486	37 477	51
102	C_8H_6	phenylacetylene	36 379	36 369[b]	52
104	C_8H_8	styrene	34 769	34 760	53
106	C_8H_{10}	*o*-xylene	37 317	37 313	54
106	C_8H_{10}	*m*-xylene	36 957	36 956	54, 55
106	C_8H_{10}	*p*-xylene	36 739	36 732	54, 56
106	C_8H_{10}	ethylbenzene	37 596	37 588	48, 52
116	C_9H_8	indene	34 736	34 730	57
118	C_9H_{10}	β-methylstyrene	34 592	34 586	58, 59
118	C_9H_{10}	indane	36 912	36 914	60
128	$C_{10}H_8$	naphthalene	32 464	32 455[c]	61
142	$C_{11}H_{10}$	phenylcyclopenta-1,3-diene	31 738	N/A	
142	$C_{11}H_{10}$	phenylcyclopenta-1,4-diene	31 687	N/A	
144	$C_{11}H_{12}$	phenylcyclo-pentene	34 646	N/A	

[a−c] In molecules where the origin is forbidden or weak, the largest vibronic band is referenced as noted: [a] 6^1_0 band of benzene, [b] 35^1_0 band of phenylacetylene, and [c] 8^1_0 band of naphthalene. [d] Assignments are based on a match-up of the entire spectrum with that found in the literature. Small differences in wavenumber positions with literature values are ascribed to calibration errors in the light sources used.

Of the spectra acquired, 15 have been assigned to specific molecular structures based on the observed vibronic structure. Whenever possible, observed transitions were compared to literature spectra and stated transition frequencies in order to make a firm assignment. In every case where a literature spectrum was used in the assignment, observed transitions were found to be within 10 cm^{-1} of that reported in absolute position and the relative spacing of transitions were within 1 cm^{-1}.

Table 1 compares the observed transitions with literature values for the origin or intense vibronic band(s).

As one can see from the table and figures, the identified species include (i) the prototypical aromatics benzene, toluene, styrene, and phenylacetylene (Figure 6); (ii) an array of aliphatic substituted benzenes (ethylbenzene; *o*-, *m*-, *p*-xylene; β-methylstyrene; Figure 7); (iii) larger fused ring structures (indene, indane, naphthalene; Figure 8a−c); and (iv) even a resonance-stabilized radical (C_7H_7, benzyl radical; Figure 8d).

In every case, single vibronic transitions had rotational band contours with widths of about 5 cm^{-1} fwhm, consistent with a significant degree of post-discharge cooling in the free jet expansion that occurs at the exit of the reaction tube. In the most intense spectra, it was possible to search sensitively for the presence of hot band transitions. When they could be seen,

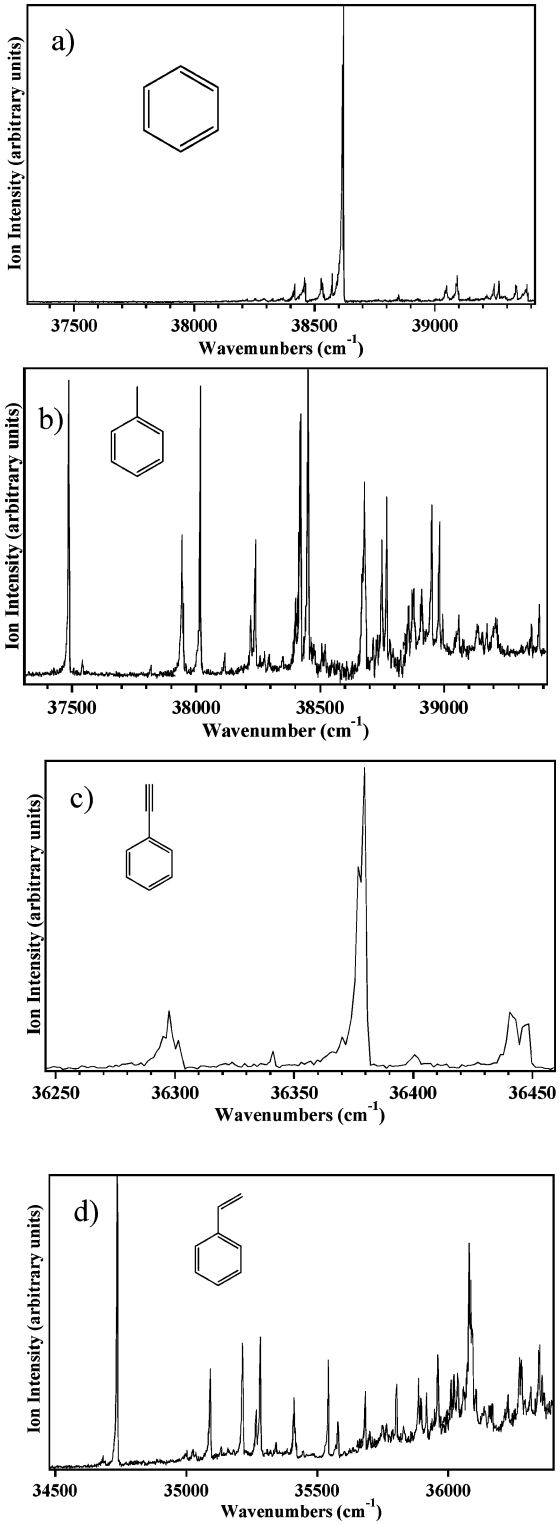

Figure 6. R2PI spectra of prototypical substituted aromatics formed in a 6% butadiene in Ar discharge: (a) benzene, (b) toluene, (c) phenylacetylene, and (d) styrene.

their intensities were very weak, indicating again that vibrational cooling is also near-complete in the post-discharge expansion.

The spectra of the molecules identified by comparison to the literature encompass the region from 32 000 to 40 000 cm^{-1}. Once an electronic origin of a product was detected, a region within 2000 cm^{-1} on either side of this origin was scanned in order to search for structural isomers. In the case of the *m*/*z* 106 product, this led to the detection of all three xylene isomers

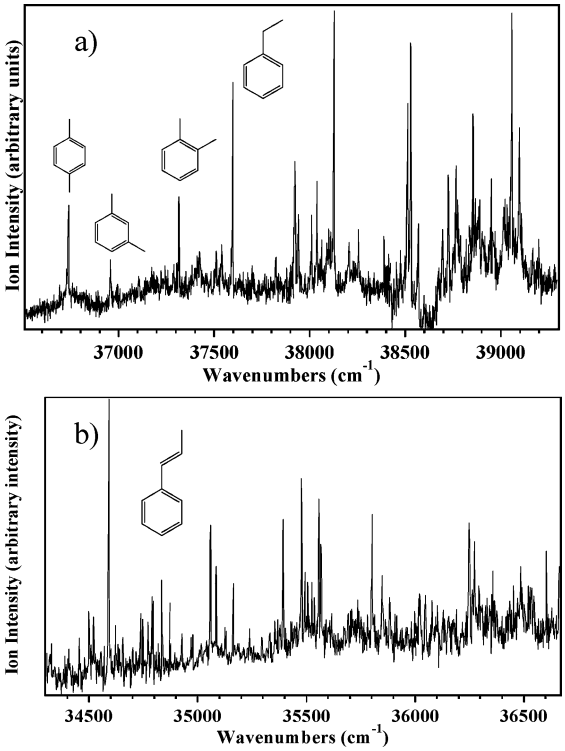

Figure 7. R2PI spectra of more highly substituted aromatics formed in a 6% butadiene in Ar discharge: (a) *o*,*m*,*p*-xylene and ethylbenzene and (b) β-methylstyrene.

(ortho, meta, para) and ethylbenzene (Figure 7), in contrast to the photochemistry, which produced ethylbenzene as the only *m*/*z* 106 product.

While most of the discharge-produced masses present in the UVMPI spectrum of Figure 5b) have even *m*/*z*, odd-mass products associated with free radicals are also observed. Some of the intensity in these mass channels may arise from fragmentation of stable molecules during the UVMPI process; however, others are due to free radicals produced by the discharge. If the free radical center is remote from the aromatic ring involved in the R2PI process, it should be possible to record R2PI spectra in the same regions as the aromatic responsible for the absorption. When recording R2PI spectra, gates were typically placed around both even and odd-mass product channels, in a certain mass region. In the 32 000−40 000 cm^{-1} region, the only sharp R2PI transitions observed in the odd-mass channels were in the $(M - 1)^+$ mass channel produced by fragmentation of the parent mass channel. However, in the case of the *m*/*z* 91 mass channel due to C_7H_7, two-color R2PI scans were recorded in the known region of the S_0-S_1 origin of the benzyl radical. The spectrum shown in Figure 8d is that of benzyl radical, indicating that free radicals are being produced by the discharge in reasonable densities.[50] We have not yet carried out extensive searches for free radicals in other wavelength regions. If the radical centers are resonance-stabilized (as in benzyl), the free radicals will have absorptions well-removed from their stable-molecule counterparts.

Several of the recorded R2PI spectra could not be assigned on the basis of comparison with literature spectra. In order to make an assignment, the most plausible structural isomers were purchased or synthesized in order to record their spectrum for comparison with the spectrum observed from the discharge. The search for molecules responsible for the observed spectral signatures was guided by the wavelength position of the electronic origin relative to that of known aromatic derivatives.

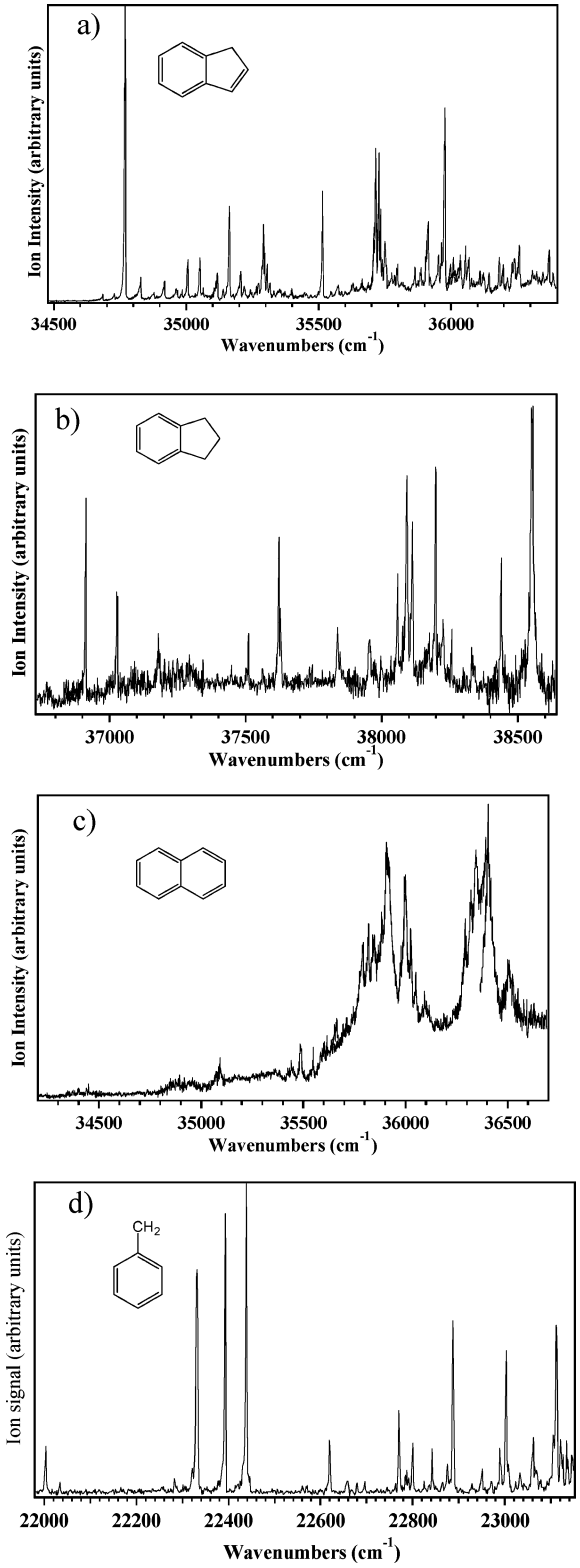

Figure 8. R2PI spectra of some fused ring and free radical products formed in a 6% butadiene in Ar discharge: (a) indene, (b) indane, (c) naphthalene, and (d) benzyl radical.

In addition, the Franck−Condon activity present in the spectrum was sometimes reminiscent of a family of aromatic derivatives, suggesting that a similar structural element could be present in the discharge product.

Figures 9 and 10 illustrate the process for the *m*/*z* 142 and 144 mass channels. The discharge-produced spectrum of *m*/*z* 142 (Figure 9a) begins at about 31 100 cm^{-1}. The origin of *m*/*z* 142 is red-shifted from the electronic origin of benzene

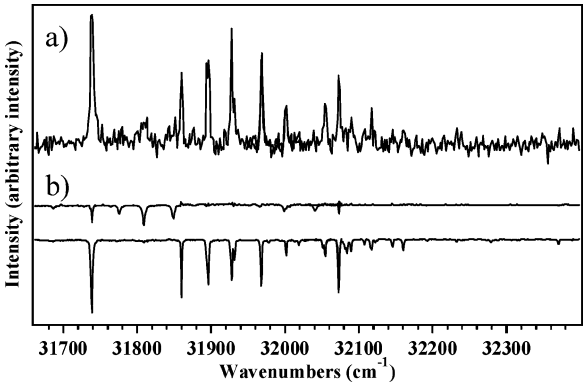

Figure 9. (a) R2PI spectrum of *m*/*z* 142 acquired from the butadiene discharge and (b) UVHB spectra of a synthesized sample of phenylcyclopentadiene (PCPD), confirming the assignment of the discharge product to PCPD and demonstrating contributions to the spectrum from two distinct isomers of the molecule.

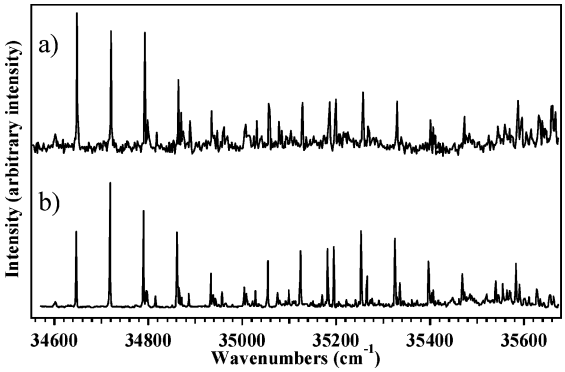

Figure 10. R2PI spectrum of *m*/*z* 144 (a) seen in the 6% butadiene in Ar discharge and (b) from a jet-cooled sample of phenylcyclopentene.

(38 086 cm^{-1})[62] by approximately 6350 cm^{-1}. By comparison, styrene has an S_0-S_1 origin at 34 760 cm^{-1},[53] 3320 cm^{-1} to the red of benzene and about half that of the *m*/*z* 142 product. A recent study of the UV spectroscopy of a total of six structural and conformational isomers of divinylbenzene removed these as candidate structures[63] but confirmed the approximate additivity of the conjugated substituents, possessing S_0-S_1 origin transitions in the range 31 408−32 621 cm^{-1}. By comparison, the S_0-S_1 origin of 1-phenyl-1,3-butadiene is at 33 315 cm^{-1},[64] well-removed from the observed spectral region.

A unique $C_{10}H_{10}$ structural isomer with two double bonds conjugated with the phenyl ring is that of phenylcyclopenta-1,3-diene. This compound was synthesized according to standard synthetic procedures.[65,66] Indeed, the expansion-cooled R2PI spectrum of this synthesized sample (Figure 9b) matched the *m*/*z* 142 discharge product spectrum (Figure 9a), providing a firm assignment for the latter. The discovery of five-membered rings in the post-discharge expansion also guided the search for the carrier of the *m*/*z* 144 spectrum. Once five-membered rings were considered as viable structures, *m*/*z* 144 was quickly identified as phenylcyclopentene (Figure 10b). The spectroscopy of these two double ring products is interesting in its own right. This *m*/*z* 142 spectrum has been observed previously in a benzene discharge but was not assigned.[41,67] We recently have also observed it in a vinylacetylene discharge,[68] indicating that the molecule is a common product in many settings. A more detailed spectroscopic characterization of these two molecules is outside of the bounds of the present investigation, but is presently being pursued. However, it is worth noting that the R2PI spectrum of phenylcyclopentadiene contains contributions from two structural isomers with different arrangements of the

TABLE 2: Summary of Product Percent Yield Data for Photolysis of 1,3-Butadiene

	193 nm[19] molecular beam, VUV detection	213.8 nm,[26] $T = 298$, gas cell, GC detection	218 nm (this work), $T \sim 75$ K, rxn tube, VUV detection (118 nm)
$C_3H_3 + CH_3$	50	dominant	60
$C_4H_5 + H$	20	NA	10
$C_4H_4 + H_2$	2	3	10
$2C_2H_3$	8	not observed	<1
$C_2H_2 + C_2H_4$	20	20	20[a]

[a] This reaction channel was not observed in these experiments, as the IP of both species is greater than 10.5 eV. This channel was estimated to be 20%, on the basis of the two previous studies (columns 1 and 2), where this channel does not appear to be sensitive to excitation energy.

double bonds in the cyclopentadiene ring relative to the position of phenyl ring attachment. The UV-hole-burning spectra in Figure 9b show the spectra of the two isomers, which have S_0-S_1 origin transitions at 31 687 and 31 738 cm^{-1}, respectively.

IV. Discussion

A. Photochemistry. *1. Primary Products.* The photodissociation of 1,3-butadiene has been studied in detail previously both under isolated molecule and room-temperature, gas-phase reaction cell conditions.[19,26] While the major emphasis of the present study is on the secondary reaction products, it is worth briefly comparing the primary product distribution observed in the present work with those that preceded it.[19,21,26] Of most direct relevance are the molecular beam photofragment translational spectroscopy data at 193 nm from Robinson et al.[19] and the study by Collin et al.[26] carried out with 213 nm UV excitation in a room-temperature, gas-phase cell. Table 2 lists the product distributions obtained in those studies and the percent product ion signals we observe. By comparison, our experiment is initiated and quenched on the 50 μs time scale following excitation at 218 nm, under bath temperature conditions of about 75 K.

The consensus from those studies[19,26] and others[20−22] is that the photodissociation of 1,3-butadiene occurs throughout this wavelength range by internal conversion to the ground state; hence, the different photoexcitation wavelengths form products with different amounts of internal energy. Since we do not have absolute VUV photoionization cross sections for all species involved, we cannot extract product quantum yields, a difficulty that was also faced in the study by Robinson et al.,[19] where product yield estimates were made on the basis of electron bombardment ionization cross sections.

The lowest energy dissociation pathway involves rearrangement via H-atom transfer to 1,2-butadiene followed by dissociation to $C_3H_3 + CH_3$.[23] In a gas cell, the 1,2-butadiene intermediate can be trapped and the competition between dissociation and stabilization has been studied. In all three studies, the $C_3H_3 + CH_3$ channel dominated the products formed.[19,26] The C_4H_5 product signal is several times smaller than the C_3H_3 signal, much as it was in the study by Robinson et al.[19] However, unlike that work, we detect the C_4H_4 product in comparable quantities to C_4H_5, while Robinson et al. find the C_4H_4 product yield to be 10 times smaller. The reason for this discrepancy is not clear, but may point to some fragmentation of the $C_4H_5^+$ into the $C_4H_4^+$ mass channel under 118 nm ionization. The lack of measurable C_2H_3 product signal in our product spectrum is consistent with its presence at 193 nm but absence at 213.8 nm (Table 2). Since the formation of two vinyl radicals is a higher-energy dissociation pathway (17 kcal/mol above the $C_3H_3 + CH_3$ limit), one anticipates a smaller percentage yield for this product at longer wavelengths.[19] Due to their high ionization thresholds, we cannot detect either the C_2H_2 or C_2H_4 products and thus are blind to the channel forming these products.

2. Secondary Reactions. In assessing plausible pathways to the other observed secondary reaction products, an initial criterion is simply whether a given reaction is exothermic or endothermic, based on known heats of formation at room temperature. A full assessment of the various pathways would require knowledge of reaction barriers; however, these are typically not available for the reactions of interest here. The heats of formation and reaction enthalpies for possible reactions producing isomeric forms of C_5H_8, C_6H_6, C_7H_7, and C_7H_8 are included in the Supporting Information. Photodissociation initially creates products that have maximum internal energies determined by the difference between the photon energy and the dissociation threshold for a given product channel. Collisional cooling with the buffer gas will equilibrate the primary products at the temperature in the reaction tube, but this will occur in competition with reaction. Since the reaction mixture is a 3−6% butadiene in argon mix, this cooling by argon should be significant prior to collision with possible reaction partners.

The dominant secondary product produced by the photochemistry of 1,3-butadiene is C_6H_6 (Figure 2b). The isotopic studies presented in section III.A prove that this product arises from propargyl recombination; however, R2PI investigations indicate that it is not benzene. This result is consistent with the detailed theoretical analysis of propargyl recombination by Miller and Klippenstein,[31] who have mapped out the minima and barriers on the C_6H_6 surface and used this surface to compute rate constants and product yields as a function of temperature and pressure under conditions relevant to combustion. The results of these calculations indicate that the product distribution is critically dependent on temperature and pressure, with benzene formation preferring low pressures and high temperatures. We do not have isomeric data on the C_6H_6 products that are formed, because the noncyclic isomers lack selective spectroscopic signatures in the ultraviolet.

The C_5H_8 product is probably 1,3-pentadiene (1,3-C_5H_8), the thermodynamically most stable pentadiene isomer that is also a methylated derivative of the 1,3-butadiene precursor. 1,3-C_5H_8 could arise from either of two pathways, involving methyl radical or C_4H_5 attack on 1,3-butadiene. Reaction 3a is slightly endothermic, and thus would require some internal energy in the methyl reactant, while 3b is exothermic, and therefore a somewhat more plausible route to C_5H_8:

$$CH_3 + C_4H_6 \rightarrow 1,3\text{-}C_5H_8 + H \quad \Delta H = +9.1 \text{ kcal/mol} \quad (3a)$$

$$C_4H_5 + C_4H_6 \rightarrow 1,3\text{-}C_5H_8 + C_3H_3 \quad \Delta H = -10.3 \text{ kcal/mol} \quad (3b)$$

Likely reactions producing C_7H_7 and C_7H_8 products involve addition of propargyl to butadiene:

$$C_3H_3 + C_4H_6 \rightarrow C_7H_7 + H_2 \quad (4a)$$

$$\rightarrow C_7H_8 + H \quad (4b)$$

However, the reactions that produce noncyclic C_7H_n products (diyne or dienyne) are endothermic by 25−40 kcal/mol. We did observe a small amount of toluene by R2PI spectroscopy (section III.A), but estimated that it was a small fraction of the

total observed C_7H_8 signal. Other cyclic C_7 products (e.g., cycloheptatriene, 2,5-norbornadiene, methylfulvene) are exothermic pathways, but these have not been probed. The corresponding reaction involving *n*-C_4H_5 attack on 1,3-butadiene can produce C_7H_7 or C_7H_8 products via loss of methane or methyl radical from the adduct:

$$n\text{-}C_4H_5 + C_4H_6 \rightarrow C_7H_7 + CH_4 \quad (5a)$$

$$\rightarrow C_7H_8 + CH_3 \quad (5b)$$

These pathways are close to thermoneutral for the noncyclic C_7 products and thus seem more probable sources of the observed C_7 signals.

Besides these major products detected by VUV photoionization, UVMPI at 266 nm was used to detect small amounts of two aromatic products at *m*/*z* 106 and 116, which were subsequently identified by R2PI spectroscopy as ethylbenzene (*m*/*z* 106) and 3-phenylpropyne (*m*/*z* 116). That these products are selectively formed is made all the more evident when searches for the *m*/*z* 106 isomers *o*-, *m*-, and *p*-xylene were also unsuccessful.

The present data is insufficient to firmly identify the pathway(s) responsible for producing these two aromatics. However, one possible mechanism for selective production of ethylbenzene is a multistep sequence in which methyl and propargyl radicals produced in the primary photodissociation subsequently recombine to form 1-butyne ($HC{\equiv}CCH_2CH_3$), which then reacts with 1,3-butadiene in a [4 + 2]-cycloaddition that produces ethylbenzene after H_2 loss:

$$1,3\text{-}C_4H_6 + h\nu\ (218\ \text{nm}) \rightarrow CH_3 + CH_2C{\equiv}CH$$

$$CH_3 + CH_2C{\equiv}CH \rightarrow [CH_3CH_2C{\equiv}CH]^{\ddagger}$$

$$[CH_3CH_2C{\equiv}CH]^{\ddagger} + 1,3\text{-}C_4H_6 \rightarrow C_6H_5CH_2CH_3 + H_2 \quad (6)$$

This series of reactions would proceed through an intermediate of 1-ethylcyclohexa-1,4-diene, which has been shown to from ethylbenzene by thermal decomposition.[69]

The C_9H_8 product identified as 3-phenylpropyne (3PP) had a reaction time profile consistent with its stature as a higher-order product. Since the side chain of 3PP is the propargyl group, it is logical to think about reactions of the propargyl radical that might produce 3PP. As a resonance-stabilized radical, many reactions of propargyl are endothermic; however, its reaction with any of the nonaromatic C_6H_6 isomers would be strongly exothermic, making the following sequence a possibility:

$$1,3\text{-}C_4H_6 + h\nu\ (218\ \text{nm}) \rightarrow CH_3 + CH_2C{\equiv}CH$$

$$2CH_2C{\equiv}CH \rightarrow C_6H_6^{\ddagger}\ (\text{nonaromatic})$$

$$C_6H_6^{\ddagger} + CH_2C{\equiv}CH \rightarrow C_6H_5CH_2C{\equiv}CH\ (3PP) + H \quad (7)$$

The presence of ethylbenzene and 3-phenylpropyne as the sole aromatic derivatives produced in the UV photochemistry of 1,3-butadiene is striking, because they appear even though benzene is not observed. While much of the attention in photochemical models of Titan's atmosphere is focused on benzene,[16,33,70] these results remind us that, under the cold conditions of Titan's atmosphere, other pathways to aromatics that do not funnel through benzene might compete with benzene as the crucial step in forming the first aromatic ring.

B. Comparing Discharge-Driven Chemistry and Photochemistry. One of the major goals of this work was to compare the products formed in an electric discharge with the photochemical products under identical conditions. Both photolysis and electric discharge excitation have been used as efficient means of producing free radicals for study. However, the chemical pathways in operation under the two circumstances are often difficult to sort out and compare.

The electric discharge differs as an excitation mechanism from a UV light source in several fundamental respects. First, electron impact is a less selective excitation scheme than photolysis, producing ions and metastable neutrals in the argon buffer gas in addition to creating neutral free radicals.

Second, aspects of the observed discharge products show a similarity with the photoproducts that may reflect similar chemical pathways in the two circumstances. For instance, the small-mass free radicals observed are C_3H_3 and CH_3, with a relative intensity similar to that formed by photolysis, indicating that the two are created in a 1:1 ratio, presumably by dissociation of 1,3-butadiene to $C_3H_3 + CH_3$, the lowest energy neutral dissociation pathway for the molecule. It is worth considering, then, whether one can understand the observed discharge products by considering neutral chemistry, especially if neutral radicals are produced in the discharge at higher concentrations than ions, as is typically thought to be the case.[71]

Third, experimental evidence indicates that the discharge conditions used in this study only reacts away a small fraction of the 1,3-butadiene. The VUV ion signals due to products of any mass were weak, with small-mass products (Figure 5a) just above the noise level and larger mass products not detectable with VUV light. At the same time, the $C_4H_6^+$ ion signal from the C_4H_6 reactant was at least 500 times the size of these discharge-generated products and was only slightly depleted by the discharge. Even this small depletion is most likely due to a discharge-induced change in the transport of the gas mixture into the ion source region.

Fourth, when UVMPI at 266 nm is used to probe the aromatic products formed by the electric discharge (Figure 5b), a much greater variety of aromatic products is observed than in photolysis (Figure 2c). Furthermore, under comparable conditions, the UVMPI mass spectra from the discharge were at least 10 times greater than those due to photolysis. This seeming contradiction between the weakness of the VUV signal and the strength and extent of the large-molecule signals seen in UVMPI may indicate that the reactions in the discharge efficiently remove the small-molecule products in favor of a wide range of larger-mass products that are thereby difficult to detect using VUV photoionization by virtue of being spread over many more mass channels.

Figure 11a depicts the molecular structures of the 1,3-butadiene discharge products we have observed and assigned in this study. The list should not be considered as an exhaustive list of the aromatics produced in the discharge, since firm assignments are limited to molecules with sharp R2PI spectra that can thereby be assigned. For comparison, Figure 11b shows the corresponding primary, secondary, and higher-order products of 1,3-butadiene photochemistry. The figure provides a ready visualization of the greater chemical processing by the discharge.

The figure also provides a summary of the relative populations of the observed products. Our intent in so doing is to stimulate ideas regarding the chemical pathways by which they are formed. One must keep in mind that the UVMPI mass spectra recorded using 266 nm have ion intensities that are affected by the presence or absence of discrete absorption bands at 266 nm.

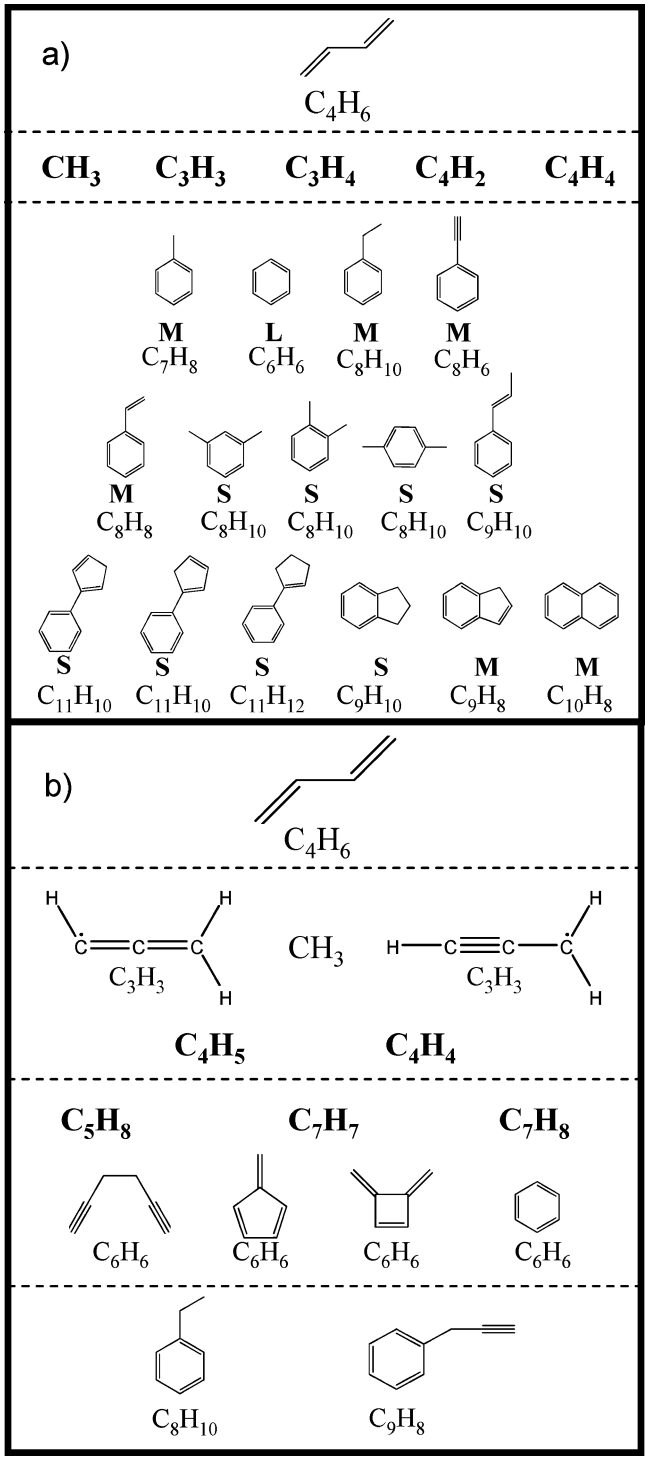

Figure 11. Summary of the molecules identified in the present study as (a) products of electric discharge of 6% butadiene in Ar with relative intensities indicated (S = small, M = medium, L = large), and (b) Primary, secondary, and higher-order products formed in 218 nm photochemistry of a 6% butadiene in helium mixture. Molecular formulas in bold denote species where structural identification was not possible.

For instance, the UVMPI intensity at *m*/*z* 106 (C_8H_{10}), *m*/*z* 128 ($C_{10}H_8$), and *m*/*z* 144 ($C_{11}H_{12}$) are distorted by the fact that ethylbenzene, naphthalene, and phenylcyclopentene have vibronic resonances or broad absorptions at 266 nm that enhance their ion signal.

A better sense for the relative populations of the discharge products can be made through comparison of the acquired R2PI spectra, taking into account the relative oscillator strengths of the transitions involved, where known. The most intense R2PI spectrum was that of benzene, with the 6^1_0 band being almost an order of magnitude more intense than any other transition recorded in the discharge experiments. This is in striking contrast to the photochemical study (section IV.A.2), which produced no measurable benzene product signal. Toluene, styrene, and indene are also observed to be strong components of the discharge, while phenylcyclopentene is not highly abundant even though it appears large in the UVMPI mass spectrum.

Since benzene is the most abundant aromatic created by the discharge, it is natural to consider how it is formed in the discharge. Suppose we prepare, as in the photochemical study, a 1:1 h_6:d_6 mixture of 1,3-butadiene. In the limit that the benzene produced in the discharge is created with complete scrambling of the isotopic composition, we would anticipate a statistical isotopic distribution of C_6H_6:C_6H_5D:$C_6H_4D_2$:$C_6H_3D_3$:$C_6H_2D_4$:C_6HD_5:C_6D_6 of 1:6:15:20:15:6:1. On the other hand, as the lowest energy pathway for butadiene fragmentation, propargyl is likely present in large abundance and could therefore be an efficient source of C_6H_6 by recombination. At the higher temperatures of the discharge, these propargyl radicals would recombine efficiently to form benzene.[33] If propargyl recombination is the sole source of the benzene, then there should be only three benzene isotopomers formed: C_6H_6, $C_6H_3D_3$, and C_6D_6. For a 1:1 h_6:d_6 mix, the relative abundances of these three products should be 1:2:1.

The results of this experiment conformed to neither limiting case. VUV was used to verify a roughly 50:50 mixture of h_6:d_6 butadiene (Figure 12a). R2PI spectra were recorded in the 6^1_0 region of benzene, monitoring all seven mass channels corresponding to the seven benzene isotopomers d_0-d_6 (*m*/*z* 78−84). The results are shown in Figure 12b. The shifts in the 6^1_0 band are those known for the different deuterated isotopes of benzene, with each deuterium contributing a shift in the 6^1_0 transition to higher frequency by ∼30 cm^{-1}.[49,72] The two dominant isotopomer products are C_6H_6 and C_6D_6, formed in a roughly 1:1 ratio, as one might anticipate if propargyl recombination dominates their formation. On the other hand, the relative intensities of the other isotopes C_6H_5D:$C_6H_4D_2$:$C_6H_3D_3$:$C_6H_2D_4$:C_6HD_5 are very close to the statistical limit expected for complete isotopic scrambling (6:15:20:15:6). The results are thus for the most part consistent with roughly equal contributions to benzene formation from statistical and propargyl recombination pathways (Figure 12c). However, the $C_6H_3D_3$ signal should have significant contributions from both mechanisms, and thus should be about three times the observed size.

One possible source of discrepancy could occur if the oscillator strength of the benzene isotopomers depended strongly on the isotopic composition. Benzene has a dipole-forbidden S_0-S_1 transition, and the 6^1_0 band is vibronically induced. However, benzene derivatives that break the 6-fold symmetry of benzene bring some allowed character to the transition. If deuterium substitution is a sufficient perturbation, it could skew the observed relative intensities of the vibronic bands. To test this possibility, we recorded 6^1_0 R2PI spectra of a 1:1 isotopic mixture of h_6:h_5d benzene. The two 6^1_0 bands appeared with equal intensity, indicating that any differences in oscillator strength are too small to explain the observed results. The photochemical results (Figure 4b), which followed the anticipated C_6H_6:$C_6H_3D_3$:C_6D_6 for propargyl recombination under those conditions, argue against a mechanistic preference during the initial propargyl recombination step. Whether the selection against $C_6H_3D_3$ could occur during isomerization on the potential energy surface leading from the propargyl recombination adduct

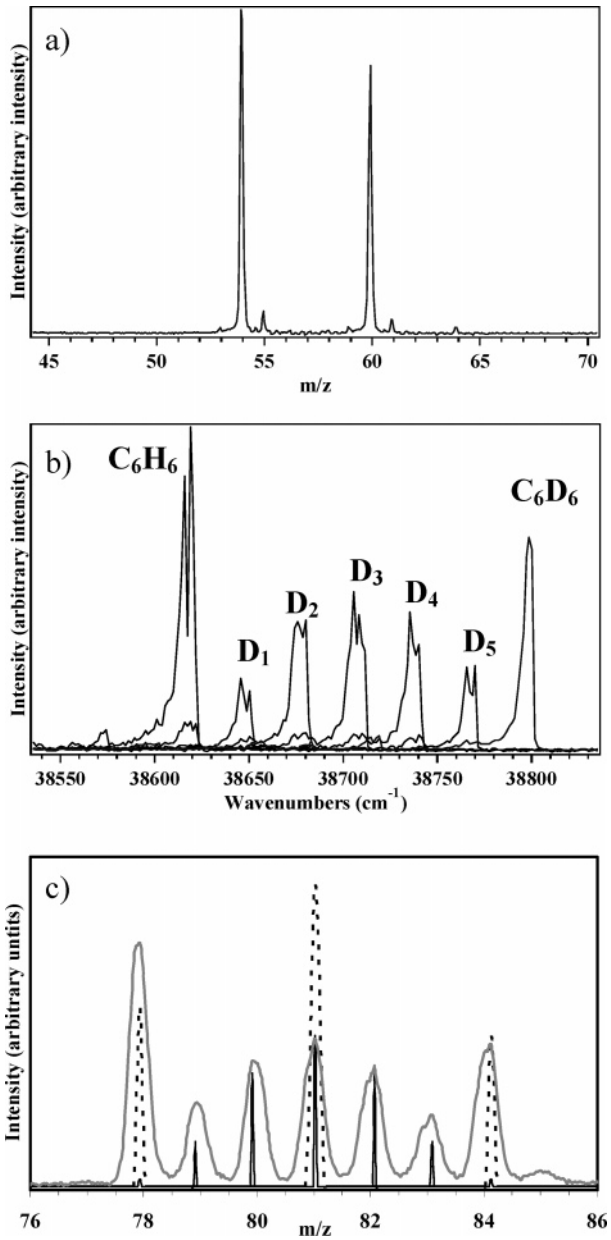

Figure 12. (a) 118 nm photoionization mass spectrum of the C_4H_6/C_4D_6 mixture of 1,3-butadiene used to study benzene formation pathways in the 6% butadiene in Ar discharge. (b) Discharge product R2PI spectra of the 6^1_0 region of benzene showing the seven isotopomers formed. (c) Overlaid mass spectra of the observed product distribution (smoothed gray) with stick diagrams showing the isotopic distribution predicted by propargyl recombination (dotted) and statistical formation (solid black).

to benzene is an intriguing but unresolved possibility. In the absence of such a resolution, we are unable to make a firm assignment of the source(s) of benzene in the discharge.

One of the distinguishing features of the discharge compared to photolysis as an excitation source is that the region in which the discharge occurs likely has a significantly higher effective temperature, thereby promoting reactions involving butadiene or its initial decomposition products (e.g., propargyl, methyl) that might be slow in the absence of this temperature increase. The observed products from the butadiene discharge (Figure 11a) show a preponderance of methylated benzenes. The presence of these products is consistent with methyl radicals formed in the initial decomposition of 1,3-butadiene adding to benzene and toluene, two of the largest population aromatics formed. Several bicyclic aromatics are also formed, among them indane, indene, and naphthalene. The five-membered rings formed in indane and indene incorporate three carbon atoms exterior to the phenyl ring, suggesting pathways involving propargyl addition to benzene. Alternatively, isomerization of 1,3-butadiene to 1,2-butadiene in the discharge could facilitate reaction with benzene to produce indene following methyl loss. The presence of naphthalene in the butadiene discharge is notable because it was *not* observed in the discharge experiments conducted by Güthe et al. on a benzene discharge, where they specifically searched for polyaromatic hydrocarbons (PAHs).[41] One might anticipate that naphthalene would be the most prevalent PAH formed in a benzene discharge. On the other hand, the pathway to naphthalene seems more circuitous starting from 1,3-butadiene, but it is observed readily. The combined results of these two studies make it clear that PAH growth in a discharge requires more than benzene alone and argues for further experiments designed to establish the most facile path from butadiene to naphthalene.

Finally, several of the products formed in the butadiene discharge do not match any previously published. In particular, the spectrum appearing in *m*/*z* 142 (Figure 9a) has been positively identified as phenylcyclopentadiene (PCPD) by comparison with the spectrum from a synthesized sample. This same spectrum was also observed in the benzene discharge of Maier[67,73] and has also been observed in a discharge of vinylacetylene in our laboratory.[68] UVHB spectroscopy (Figure 9b) was used to determine that there were two isomers of PCPD present, one of which is more intense than the other by almost a factor of 10. A recent study by Bernard-Henriet determined that, at room temperature, phenylcyclopenta-1,3-diene is thermodynamically favored over phenylcyclopenta-1,4-diene by a 7:1 ratio.[65] On this basis, we make a tentative assignment of the more intense spectrum to phenylcyclopenta-1,3-diene and the less intense one to the 1,4-diene isomer. The isomer-specific spectroscopy of these two isomers is currently being explored and will be published elsewhere.[74]

The assignment of the carrier of the *m*/*z* 142 spectrum to phenylcyclopentadiene also guided the search for candidates for the R2PI spectrum appearing in the *m*/*z* 144 mass channel. Initially, phenyl derivatives containing a five-membered ring were not considered. However, the positive identification of the *m*/*z* 142 spectrum to phenylcyclopentadiene made the assignment of the *m*/*z* 144 spectrum to phenylcyclopentene straightforward. The S_0-S_1 electronic origin of the *m*/*z* 144 spectrum is in the same region as styrene, indicating that there must be a double bond conjugated to the benzene ring. Comparison with the spectrum of a commercially available sample confirmed the assignment.

The present data do not provide a definite answer to the important question of how these molecules are formed in the discharge. Given the important role played by the propargyl radical as the lowest energy decomposition pathway of 1,3-butadiene, a plausible final step could involve propargyl addition to phenylacetylene to produce the phenylcyclopentadienyl radical, which can subsequently form phenylcyclopentadiene after H-atom addition (Figure 13). Support for such a pathway motivates further studies of propargyl reactions with benzene derivatives.

The fact that these bicyclic compounds containing five-membered rings were found as products of discharges of butadiene, vinylacetylene, and benzene suggests that there may be a particularly facile route to their production. The UV spectra of these compounds lay a foundation for their identification in

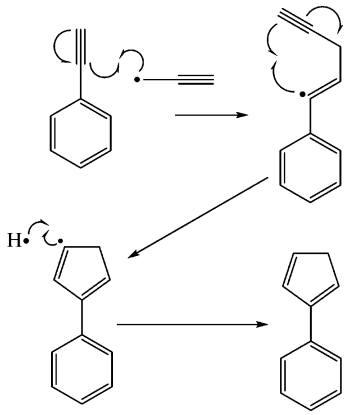

Figure 13. Proposed reaction scheme for production of phenylcyclopentadiene in the butadiene discharge.

other environments. It will be important to study the isomer-specific spectroscopy, energetics, and formation pathways of these molecules, which could play a role not only in Titan's atmosphere but also in a wide range of other settings including combustion.

V. Conclusion

The present study has compared the photochemical and discharge-driven pathways that lead from 1,3-butadiene to aromatic products. The only observed aromatic photochemical products are ethylbenzene and 3-phenylpropyne (Figure 11b), while some 15 aromatic products were observed and identified in the butadiene discharge (Figure 11a). In many cases, plausible pathways to these products have been proposed; however, much more work using a range of complementary methods is required before these pathways can be considered established with confidence. Nevertheless, future studies of the photochemical and discharge-driven pathways in other unsaturated hydrocarbons are warranted. The present work has also highlighted the role that can be played by isotopic labeling studies as a general tool for sorting mechanisms. In addition, plausible pathways to a given product can be explored via doping studies that add a small amount of a proposed intermediate to the discharge in order to see which products are thereby enhanced.

Acknowledgment. The authors gratefully acknowledge support from the NASA Planetary Atmospheres Program (NNG06GC57G) for this research.

Supporting Information Available: Tables of the thermodynamic data used in the product analysis. This material is available free of charge via the Internet at http://pubs.acs.org.

References and Notes

(1) Courtin, R.; Wagener, R.; McKay, C. P.; Caldwell, J.; Fricke, K. H.; Raulin, F.; Bruston, P. *Icarus* **1991**, *90*, 43.
(2) Raulin, F.; Owen, T. *Space Sci. Rev.* **2002**, *104*, 377.
(3) Clarke, D. W.; Ferris, J. P. *Icarus* **1997**, *127*, 158.
(4) Tran, B. N.; Joseph, J. C.; Ferris, J. P.; Persans, P. D.; Chera, J. J. *Icarus* **2003**, *165*, 379.
(5) Trainer, M. G.; Pavlov, A. A.; Jimenez, J. L.; McKay, C. P.; Worsnop, D. R.; Toon, O. B.; Tolbert, M. A. *Geophys. Res. Lett.* **2004**, *31*.
(6) Clarke, D. W.; Ferris, J. P. *Origins Life Evol. Biosphere* **1997**, *27*, 225.
(7) Sagan, C.; Reid Thompson, W. *Icarus* **1984**, *59*, 133.
(8) Flasar, F. M.; Achterberg, R. K.; Conrath, B. J.; Gierasch, P. J.; Kunde, V. G.; Nixon, C. A.; Bjoraker, G. L.; Jennings, D. E.; Romani, P. N.; Simon-Miller, A. A.; Bezard, B.; Coustenis, A.; Irwin, P. G. J.; Teanby, N. A.; Brasunas, J.; Pearl, J. C.; Segura, M. E.; Carlson, R. C.; Mamoutkine, A.; Schinder, P. J.; Barucci, A.; Courtin, R.; Fouchet, T.; Gautier, D.; Lellouch, E.; Marten, A.; Prange, R.; Vinatier, S.; Strobel, D. F.; Calcutt, S. B.; Read, P. L.; Taylor, F. W.; Bowles, N.; Samuelson, R. E.; Orton, G. S.; Spilker, L. J.; Owen, T. C.; Spencer, J. R.; Showalter, M. R.; Ferrari, C.; Abbas, M. M.; Raulin, F.; Edgington, S.; Ade, P.; Wishnow, E. H. *Science* **2005**, *308*, 975.
(9) Tomasko, M. G.; Archinal, B.; Becker, T.; Bezard, B.; Bushroe, M.; Combes, M.; Cook, D.; Coustenis, A.; de Bergh, C.; Dafoe, L. E.; Doose, L.; Doute, S.; Eibl, A.; Engel, S.; Gliem, F.; Grieger, B.; Holso, K.; Howington-Kraus, E.; Karkoschka, E.; Keller, H. U.; Kirk, R.; Kramm, R.; Kuppers, M.; Lanagan, P.; Lellouch, E.; Lemmon, M.; Lunine, J.; McFarlane, E.; Moores, J.; Prout, G. M.; Rizk, B.; Rosiek, M.; Rueffer, P.; Schroder, S. E.; Schmitt, B.; See, C.; Smith, P.; Soderblom, L.; Thomas, N.; West, R. *Nature* **2005**, *438*, 765.
(10) Griffith, C. A.; Penteado, P.; Rannou, P.; Brown, R.; Boudon, V.; Baines, K. H.; Clark, R.; Drossart, P.; Buratti, B.; Nicholson, P.; McKay, C. P.; Coustenis, A.; Negrao, A.; Jaumann, R. *Science* **2006**, *313*, 1620.
(11) Rannou, P.; Montmessin, F.; Hourdin, F.; Lebonnois, S. *Science* **2006**, *311*, 201.
(12) Atreya, S. *Science* **2007**, *316*, 843.
(13) Toublanc, D.; Parisot, J. P.; Brillet, J.; Gautier, D.; Raulin, F.; McKay, C. P. *Icarus* **1995**, *113*, 2.
(14) Wilson, E. H.; Atreya, S. K. *Planetary Space Sci.* **2003**, *51*, 1017.
(15) Wilson, E. H.; Atreya, S. K. *J. Geophys. Res.—Planets* **2004**, *109*.
(16) Wilson, E. H.; Atreya, S. K.; Coustenis, A. *J. Geophys. Res.—Planets* **2003**, *108*.
(17) Niemann, H. B.; Atreya, S. K.; Bauer, S. J.; Carignan, G. R.; Demick, J. E.; Frost, R. L.; Gautier, D.; Haberman, J. A.; Harpold, D. N.; Hunten, D. M.; Israel, G.; Lunine, J. I.; Kasprzak, W. T.; Owen, T. C.; Paulkovich, M.; Raulin, F.; Raaen, E.; Way, S. H. *Nature* **2005**, *438*, 779.
(18) Waite, J. H.; Young, D. T.; Cravens, T. E.; Coates, A. J.; Crary, F. J.; Magee, B.; Westlake, J. *Science* **2007**, *316*, 870.
(19) Robinson, J. C.; Harris, S. A.; Sun, W. Z.; Sveum, N. E.; Neumark, D. M. *J. Am. Chem. Soc.* **2002**, *124*, 10211.
(20) Robinson, J. C.; Sun, W. Z.; Harris, S. A.; Qi, F.; Neumark, D. M. *J. Chem. Phys.* **2001**, *115*, 8359.
(21) Mu, X.; Lu, I.-C.; Shih-Huang, L.; Wang, X.; Yang, X. *J. Phys. Chem. A* **2004**, *108*, 11470.
(22) Chambreau, S. A.; Lemieux, J.; Wang, L. M.; Zhang, J. S. *J. Phys. Chem. A* **2005**, *109*, 2190.
(23) Lee, H. Y.; Kislov, V. V.; Lin, S. H.; Mebel, A. M.; Neumark, D. M. *Chem.—Eur. J.* **2003**, *9*, 726.
(24) Arrington, C. A.; Ramos, C.; Robinson, A. D.; Zwier, T. S. *J. Phys. Chem. A* **1998**, *102*, 3315.
(25) Srinivasan, R. *J. Am. Chem. Soc.* **1960**, *82*, 5063.
(26) Collin, G. J.; Deslauriers, H.; Demare, G. R.; Poirier, R. A. *J. Phys. Chem.* **1990**, *94*, 134.
(27) Fulchignoni, M.; Ferri, F.; Angrilli, F.; Ball, A. J.; Bar-Nun, A.; Barucci, M. A.; Bettanini, C.; Bianchini, G.; Borucki, W.; Colombatti, G.; Coradini, M.; Coustenis, A.; Debei, S.; Falkner, P.; Fanti, G.; Flamini, E.; Gaborit, V.; Grard, R.; Hamelin, M.; Harri, A. M.; Hathi, B.; Jernej, I.; Leese, M. R.; Lehto, A.; Stoppato, P. F. L.; Lopez-Moreno, J. J.; Makinen, T.; McDonnell, J. A. M.; McKay, C. P.; Molina-Cuberos, G.; Neubauer, F. M.; Pirronello, V.; Rodrigo, R.; Saggin, B.; Schwingenschuh, K.; Seiff, A.; Simoes, F.; Svedhem, H.; Tokano, T.; Towner, M. C.; Trautner, R.; Withers, P.; Zarnecki, J. C. *Nature* **2005**, *438*, 785.
(28) Bandy, R. E.; Lakshminarayan, C.; Frost, R. K.; Zwier, T. S. *Science* **1992**, *258*, 1630.
(29) Bandy, R. E.; Lakshminarayan, C.; Frost, R. K.; Zwier, T. S. *J. Chem. Phys.* **1993**, *98*, 5362.
(30) Zwier, T. S.; Allen, M. *Icarus* **1996**, *123*, 578.
(31) Miller, J. A.; Klippenstein, S. J. *J. Phys. Chem. A* **2001**, *105*, 7254.
(32) Miller, J. A.; Klippenstein, S. J. *J. Phys. Chem. A* **2003**, *107*, 7783.
(33) Shafir, E. V.; Slagle, I. R.; Knyazev, V. A. *J. Phys. Chem. A* **2003**, *107*, 8893.
(34) Khare, B. N.; Bakes, E. L. O.; Imanaka, H.; McKay, C. P.; Cruikshank, D. P.; Arakawa, E. T. *Icarus* **2002**, *160*, 172.
(35) Khare, B. N.; Sagan, C.; Zumberge, J. E.; Sklarew, D. S.; Nagy, B. *Icarus* **1981**, *48*, 290.
(36) Imanaka, H.; Khare, B. N.; Elsila, J. E.; Bakes, E. L. O.; McKay, C. P.; Cruikshank, D. P.; Sugita, S.; Matsui, T.; Zare, R. N. *Icarus* **2004**, *168*, 344.
(37) Frost, R. K.; Zavarin, G. S.; Zwier, T. S. *J. Phys. Chem.* **1995**, *99*, 9408.
(38) Stearns, J. A.; Zwier, T. S.; Kraka, E.; Cremer, D. *Phys. Chem. Chem. Phys.* **2006**, *8*, 5317.
(39) Xin, J.; Fan, H. Y.; Ionescu, I.; Annesley, C.; Reid, S. A. *J. Mol. Spectrosc.* **2003**, *219*, 37.
(40) Harper, W. W.; Clouthier, D. J. *J. Chem. Phys.* **1997**, *106*, 9461.
(41) Güthe, F.; Ding, H. B.; Pino, T.; Maier, J. P. *Chem. Phys.* **2001**, *269*, 347.
(42) Vlasak, P. R.; Beussman, D. J.; Davenport, M. R.; Enker, C. G. *Rev. Sci. Instrum.* **1996**, *67*, 68.
(43) Mahon, R.; McIlrath, T. J.; Myerscough, V. P.; Koopman, D. W. *IEEE J. Quantum Electron.* **1979**, *15*, 444.

(44) Robinson, J. C.; Sveum, N. E.; Neumark, D. M. *J. Chem. Phys.* **2003**, *119*, 5311.
(45) Leopold, D. G.; Pendley, R. D.; Roebber, J. L.; Hemley, R. J.; Vaida, V. *J. Chem. Phys.* **1984**, *81*, 4218.
(46) Harman, P. J.; Kent, J. E.; Odwyer, M. F.; Griffith, D. W. T. *J. Phys. Chem.* **1981**, *85*, 2731.
(47) Kent, J. E.; Harman, P. J.; Odwyer, M. F. *J. Phys. Chem.* **1981**, *85*, 2726.
(48) Breen, P. J.; Bernstein, E. R.; Seeman, J. I. *J. Chem. Phys.* **1987**, *87*, 3269.
(49) Garforth, F. M.; Ingold, C. K. *J. Chem. Soc.* **1948**, 417.
(50) Fukushima, M.; Obi, K. *J. Chem. Phys.* **1990**, *93*, 8488.
(51) Hickman, C. G.; Gascooke, J. R.; Lawrance, W. D. *J. Chem. Phys.* **1996**, *104*, 4887.
(52) King, G. W.; So, S. P. *J. Mol. Spectrosc.* **1970**, *36*, 468.
(53) Syage, J. A.; Aladel, F.; Zewail, A. H. *Chem. Phys. Lett.* **1983**, *103*, 15.
(54) Breen, P. J.; Warren, J. A.; Bernstein, E. R.; Seeman, J. I. *J. Chem. Phys.* **1987**, *87*, 1917.
(55) Zhang, S.; Tang, B. F.; Wang, Y. M.; Zhang, B. *Chem. Phys. Lett.* **2004**, *397*, 495.
(56) Walter, K.; Scherm, K.; Boesl, U. *Chem. Phys. Lett.* **1989**, *161*, 473.
(57) Kendler, S.; Zilberg, S.; Haas, Y. *Chem. Phys. Lett.* **1995**, *242*, 139.
(58) Kendler, S.; Haas, Y. *Chem. Phys. Lett.* **1995**, *236*, 324.
(59) Sinclair, W. E.; Yu, H.; Phillips, D.; Gordon, R. D.; Hollas, J. M.; Klee, S.; Mellau, G. *J. Phys. Chem.* **1995**, *99*, 4386.
(60) He, Y. G.; Kong, W. *J. Chem. Phys.* **2005**, *122*, 244302.
(61) Beck, S. M.; Powers, D. E.; Hopkins, J. B.; Smalley, R. E. *J. Chem. Phys.* **1980**, *73*, 2019.
(62) Sur, A.; Knee, J.; Johnson, P. *J. Chem. Phys.* **1982**, *77*, 654.
(63) Selby, T. M.; Meerts, W. L.; Zwier, T. S. *J. Phys. Chem. A* **2007**, *111*, 3697.
(64) Buma, W. J.; Kohler, B. E.; Nuss, J. M.; Shaler, T. A.; Song, K. *J. Chem. Phys.* **1992**, *96*, 4860.
(65) Bernard-Henriet, C.; Chanon, M. *Tetrahedron Lett.* **1996**, *37*, 2417.
(66) Riemschneider, R.; Nehring, R. *Monatsh. Chem.* **1960**, *91*, 829.
(67) Schmidt, T. W. Personal communication **2006**.
(68) Newby, J. J.; Liu, C.-P.; Zwier, T. S. Unpublished results.
(69) Cocks, A. T.; Hopkins, R. G.; Frey, H. M. *J. Chem. Soc.-Faraday Trans.1* **1972**, *68*, 1287.
(70) Tang, W. Y.; Tranter, R. S.; Brezinsky, K. *J. Phys. Chem. A* **2005**, *109*, 6056.
(71) Anderson, D. T.; Davis, S.; Zwier, T. S.; Nesbitt, D. J. *Chem. Phys. Letters* **1996**, *258*, 207.
(72) Garforth, F. M.; Ingold, C. K. *J. Chem. Soc.* **1948**, 483.
(73) Yin, H. M.; Heazlewood, B. R.; Stamford, N. P. J.; Nauta, K.; Bacskay, G. B.; Kable, S. H.; Schmidt, T. W. *J. Phys. Chem. A* **2007**, *111*, 3306.
(74) Newby, J. J.; Liu, C.-P.; Müller, C.; Zwier, T. S. In preparation.